Nuclear Inst. and Methods in Physics Research, A 979 (2020) 164494

Contents lists available at ScienceDirect

Nuclear Inst. and Methods in Physics Research, A

journal homepage: www.elsevier.com/locate/nima

Study of interpad-gap of HPK 3.1 production LGADs with Transient Current Technique☆

S. Bharthuar [a,b,*], J. Ott [a,d], K. Helariutta [c], V. Litichevskyi [a,b], E. Brücken [a,b], A. Gädda [a], L. Martikainen [a,b], S. Kirschenmann [a,b], T. Naaranoja [a,b], P. Luukka [a,e]

[a] Helsinki Institute of Physics, Gustaf Hällströmin katu 2, FI-00014, Finland
[b] Department of Physics, University of Helsinki, Gustaf Hällströmin katu 2, FI-00014, Finland
[c] Department of Chemistry, University of Helsinki, A.I. Virtasen aukio 1, FI-00560, Finland
[d] Aalto University, Department of Electronics and Nanoengineering, Tietotie 3, Espoo, FI-02150, Finland
[e] Lappeenranta-Lahti University of Technology, Yliopistonkatu 34, Lappeenranta, FI-53850, Finland

ARTICLE INFO

Keywords:
Low gain avalanche detector (LGAD)
Scanning-TCT
Fill factor

ABSTRACT

The Phase-2 upgrade of the Large Hadron Collider (LHC) to High-Luminosity LHC (HL-LHC) allows an increase in the operational luminosity value by a factor of 5–7 that will result in delivering 3000 fb^{-1} or more integrated luminosity. Due to high luminosity, the number of interactions per bunch crossings (pileup) will increase up to a value of 140–200. To cope with high pileup rates, a precision minimum ionising particles (MIPs) timing detector (MTD) with a time resolution of ∼30–40 ps and hermetic coverage up to a pseudo-rapidity of $|\eta| = 3$ is proposed by the Compact Muon Solenoid (CMS) experiment. An endcap part ($1.6 < |\eta| < 3$) of the MTD, called the endcap timing layer, will be based on low-gain avalanche detector (LGAD) technology. LGADs provide a good timing resolution due to a combination of a fast signal rise time and high signal-to-noise ratio. The performance of the ETL depends on optimising the crucial features of the sensors, namely; gain, signal homogeneity, fill factor, leakage current, uniformity of multiple-pad sensors and long term stability. The paper mainly focuses on the study of the fill factor of LGADs with varying temperature and irradiation at varying proton fluences as these sensors will be operated at low temperatures and are subjected to a high radiation environment.

The 3.1 production of LGADs from Hamamatsu Photonics K.K. (HPK) includes 2x2 sensors with different structures, in particular, different values of narrower inactive region widths between the pads, called the no-gain region. In this paper, the term interpad-gap is used instead of no-gain region in order to follow the conventional terminology. These sensors have been designed to study their fill factor, which is the ratio of the area within the active region (gain region) to the total sensor area. A comparative study on the dependence of breakdown voltage with the interpad-gap width for the sensors has been carried out. Using infrared light (as the electron–hole pair creation by IR laser mimics closely to the traversing of MIPs) from the Scanning-Transient Current Technique (Scanning-TCT) set-up shows that the fill factor does not vary significantly with a variation in temperature and irradiation at high proton fluences.

1. Introduction

The High Luminosity Large Hadron Collider (HL-LHC) run, also known as the Phase-2 operation of the LHC, will start after Long Shutdown 3 (LS3). During the HL-LHC phase, the number of interactions per bunch crossing (pileup) will increase to an average value of 140, corresponding to a nominal luminosity of 5.0×10^{34} cm^{-2}s^{-1}. The amount of collected data corresponding to an integrated luminosity of 3000 fb^{-1}, will increase the precision of the Standard Model measurements, such as, the search for di-Higgs production and direct measurement of the Higgs self coupling which is one of the main priorities of the HL-LHC physics program. The HL-LHC will also increase the sensitivity for Beyond Standard Model searches, such as, electroweak SUSY chargino–neutralino production [1]. Due to increased pileup, the spatial overlapping of the tracks and energy deposition will cause a degradation in the particle identification and reconstruction of the tracks during the hard *pp* interaction. Therefore, the upgraded detector must be able to survive and function efficiently in the harsh radiation environment.

☆ On behalf of the CMS Collaboration.

* Corresponding author at: Helsinki Institute of Physics, Gustaf Hällströmin katu 2, FI-00014, Finland.
E-mail address: shudhashil.bharthuar@helsinki.fi (S. Bharthuar).

https://doi.org/10.1016/j.nima.2020.164494
Received 28 February 2020; Received in revised form 22 July 2020; Accepted 28 July 2020
Available online 3 August 2020

In the upgrade plan for the HL-LHC run, the Compact Muon Solenoid (CMS) experiment will install a precision minimum ionising particles timing detector (MTD) to measure ionising particles with a time resolution of nearly 30–40 ps, degrading slowly to a magnitude of 50–60 ps due to radiation damage. The MTD will allow time of arrival (ToA) measurements that can separate the collisions very close in space as well as in time with a hermetic angular coverage up to a pseudo-rapidity of $|\eta| = 3$ [2].

The MTD is located between the tracker and the electromagnetic calorimeter of the CMS experiment. It will consist of a barrel ($|\eta| < 1.5$) and an endcap part ($1.6 < |\eta| < 3$), as shown in Fig. 1. The endcap part of the MTD, known as the endcap timing layer (ETL), will be based on low gain avalanche detector (LGAD) technology.

Fig. 2 shows the cross-sectional view of the active thickness of an LGAD (without the support wafer). The high electric field region in the moderately doped p-implant allows impact ionisation which gives rise to the multiplication of charge carriers generated within the bulk of the detector. This multiplication process provides the gain to the detector; therefore, the p-implant is also known as the gain/multiplication layer. The gain provides a fast signal rise time with a good timing resolution, as well as a sufficiently high signal even after irradiation. The area under the multiplication layer consists of a full-gain region and a small transition region. The full-gain region is the area under the multiplication layer that corresponds to a high and uniform electric field within a fully depleted bulk. The transition region corresponds to the low electric field section within the p^--substrate of the detector [4]. The no-gain region is the distance between the gain region of the two adjacent pads of the sensor. The no-gain region consists of deep n-doped implants, called junction terminal extension (JTE), at the edges surrounded by a p-stop implant to improve the breakdown behaviour of the detector.

As per the convention, the authors have used the term interpad-gap instead of no-gain region. There are two interpad-gap values. One is the nominal interpad-gap and the second is the measured interpad-gap. The nominal interpad-gap refers to the actual distance between the gain region of the adjacent pads as per the actual design layout of the sensors. The measured interpad-gap is the actual effective value we obtain by measuring with the help of the IR laser in the scanning-TCT set-up.

The timing resolution and performance of the ETL depend upon the design of the sensor. These objectives can be achieved by studying and optimising some of the crucial features of the LGADs, which are: (i) high gain and low noise as the sensors must provide large signals in order to have an excellent timing resolution, (ii) high fill factor to increase the number of two hit tracks, (iii) wafer uniformity, quality of multi-pad sensors and single pad leakage current to ensure that all sensors have the same gain and provide uniform charge collection efficiency, and therefore an equal timing resolution, (iv) a high hit efficiency which can be achieved only if the gain is uniform within the individual pads and the signal is uniform across the whole sensor, so that all hits are above the threshold, and (v) a long-term stability since the stability of the sensors may be affected by annealing effects [5].

In this paper, the authors have focused on the study of fill factor, which is the ratio of the active area (= area of gain region) and the total sensor area. This value can be less than 100% due to the edge width and the no-gain region between the adjacent pads within the sensor (shown in Fig. 2).

The 3.1 production batch LGADs provided by one of the vendors, Hamamatsu Photonics K.K (HPK), have been studied in this paper. The specification of the samples are described in Section 2. The sensor geometry plays a significant role in determining the fill factor, which in turn affects the efficiency and the performance of the detector. The fill factor depends upon the active area (gain region) of the sensor. Therefore, there is a need to optimise the active area of the sensor which is affected by the nominal interpad-gap. Further, the design of the gain termination region also affects the breakdown voltage of the sensor (shown in Section 3.1). Therefore, the aim of the study is to investigate the geometry of the sensors, specifically the nominal interpad-gap.

Furthermore, since the gain of these sensors depends upon temperature and proton fluence of irradiation, the measured interpad-gap and fill factor have been studied with these varying factors by using the Scanning Transient Current Technique (TCT) set-up (shown in Section 3.2).

2. Samples measured

The samples measured are LGADs from the HPK 3.1 production batch. The design of the sensors studied are mentioned in the 2019 CMS MTD Technical Proposal (TP) [2]. The thickness of the active p-type bulk (p^--substrate shown in Fig. 2) region of the sensors is 50 μm. As shown in Fig. 3, the sensors have four pads (2 × 2) with a common guard ring around them. Each of the pads has an area of 1 × 3 mm^2. The samples differ in their nominal interpad-gap values.

The nominal values of interpad-gap are 30, 50, 70 and 95 μm, respectively. The sensors have been categorised into two types: Type A and Type B on the basis of the presence of a broad metallisation area above the active region of the sensor (as shown in Fig. 3).

3. Measurements

3.1. IV–CV measurements

Capacitance versus voltage (CV) and current versus voltage (IV) measurements were performed at the probe station in the Detector Laboratory of the Helsinki Institute of Physics, Finland.

For IV measurements, bias voltage is provided to the back-plane of the sensor through the probe station chuck by the Keithley 2410-C SourceMeter, which can provide voltage within the range of ± 1000 V. A Keithley 6487 picoammeter is used to measure the pad current through a probe needle attached to the pad of the sensor while Keithley 2410-C SourceMeter is used to measure the total current of the device.

For CV measurements, the device was connected by a probe needle through an isobox that couples the signal from an Agilent E4980A Precision LCR meter to the high bias voltage, supplied by Keithley 2410-C, and filters the bias voltage out of the capacitance meter. Capacitances were recorded at an AC frequency of 10 kHz. The plot for the inverse of square capacitance versus voltage from CV measurements shows that the full depletion voltage of the gain layer (V_{GL}) and the entire bulk of the detector (V_{FD}) are of a magnitude of 38 V and 49 V, respectively (shown in Fig. 4).

IV measurements of type A and B sensors with varying nominal interpad-gaps were performed in two different modes depending upon the floating/grounding configuration of the remaining pads while current was read out from one of the pads (shown in Fig. 5). The sensors have a breakdown voltage of 220 V. The breakdown voltage is independent of the floating and/or grounding configuration of the remaining pads for sensors with 50, 70 and 95 μm nominal interpad-gap; but is not the same for the ones with 30 μm nominal interpad-gap. It is clear from Fig. 5a that the sensor with 30 μm nominal interpad-gap has a breakdown voltage of about 120 V if the remaining pads are floating. This shows that the breakdown voltage is dependent upon the design of the gain termination region and the nominal interpad-gap value. The gain termination region consists of the edge termination and the peripheral regions. As a consequence of the fabrication process, at a high operational reverse bias voltage, the electrostatic potential increases at the n^+-p junction edge which causes a local increase of the electric field in this region. The edge termination region consists of the JTE which lowers the electric field at the n^+-p junction curvature and ensures a uniform electric field profile at the edges of the active region of the detector. Further, after fabrication, the field oxide contains a certain concentration of positive oxide charges within its

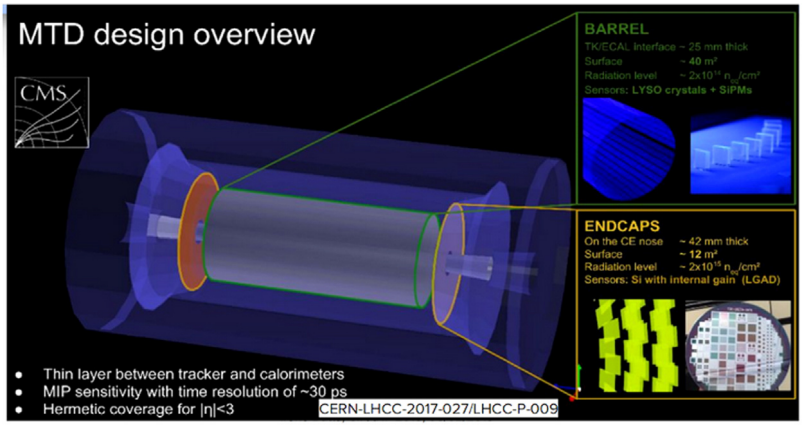

Fig. 1. CMS MTD design layout showing the positioning of its barrel and endcap part [3].

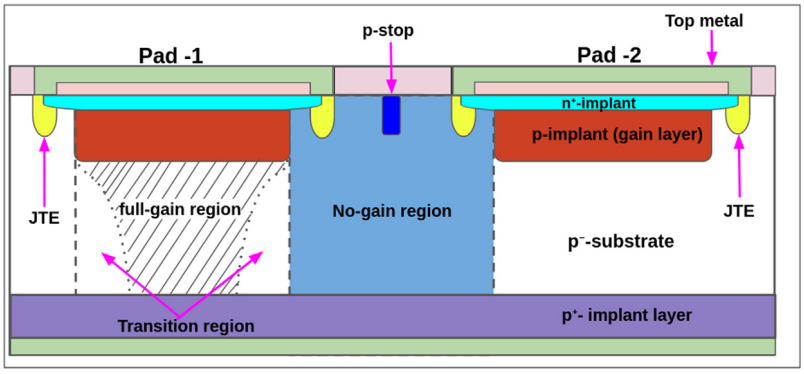

Fig. 2. Cross-sectional view of the active thickness (without support wafer) illustrating the gain and no-gain regions across two adjacent pads of an LGAD.

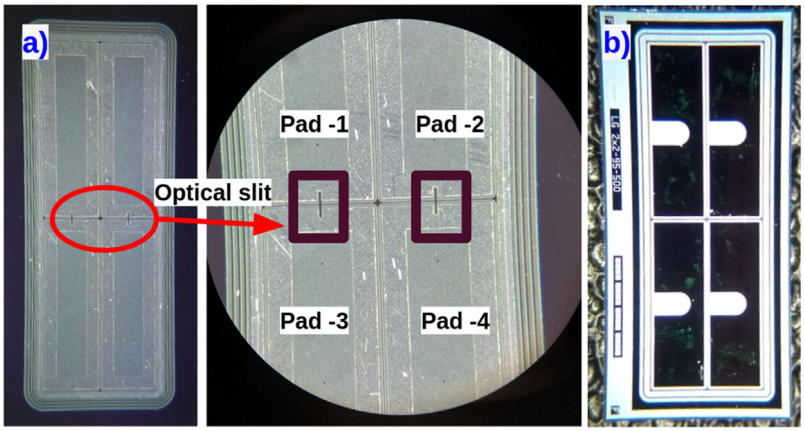

Fig. 3. HPK 3.1 production sample with 2×2 pads showing sensors (a) with broader metallisation region on pads and small optical slit running across adjacent pads (Type A) and (b) individual pads with wider optical opening (Type B).

volume, which induces an accumulation of negative charges at the surface of the peripheral region. This subsequently generates a shallow inversion layer in the low doped p^--substrate which is responsible for the increase in surface currents. However, the p-stop implant in the peripheral region provides a solution to eliminate the surface current path by preventing an accumulation of negative charges [6]. Therefore, the optimum electrical performance of LGADs requires, apart from an accurate control of the multiplication layer, a careful optimisation of the edge termination and peripheral regions in order to make sure that there is no premature breakdown or rise in the surface leakage current levels.

It also shows that the grounding of adjacent pads is crucial in order to avoid very early breakdown for sensors with narrower nominal interpad-gap. In practical operation, the metallic contacts over the individual pads and the guard rings of the sensors would be bump-bonded to the read-out chip (ROC). The electrical connection for each sensor is such that the guard ring is grounded while each of the pads is terminated as they are bump-bonded to the ROC amplifier input which provides a virtual ground to the individual pads. If there are any dead bump-bonds, it would mean that the pads will be left floating. Therefore, it is relevant to check whether the breakdown voltage is affected if the pads are in grounding/floating mode configuration; especially since all the pads are read out simultaneously. Further, Fig. 5a and b

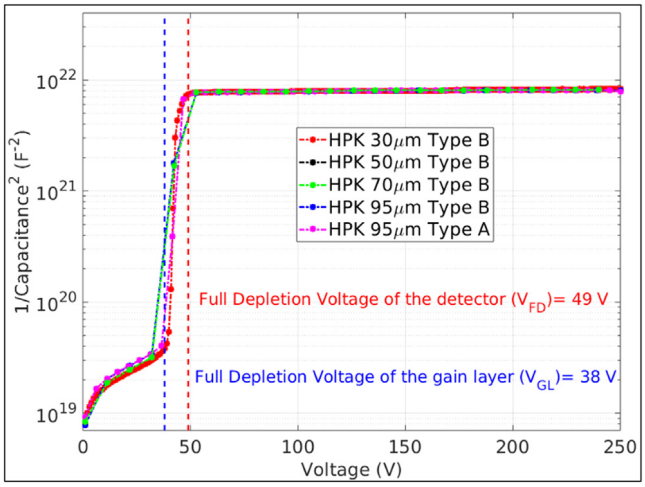

Fig. 4. Capacitance^{-2} versus voltage plots for HPK 3.1 production sensors showing the determination of the full depletion voltage of the gain layer and the entire bulk of the sensors with different nominal interpad-gaps.

show that, irrespective of the floating/grounding configuration of the adjacent pads, the breakdown voltage is not dependent on the presence of a broad metallisation over the active region of the sensor.

3.2. Scanning-transient current technique measurements

TCT is a method commonly used for electrical characterisation of semiconductor detectors. In TCT, a fast pulsed IR laser is used to imitate the crossing of MIPs through the detector [7]. The current induced by this pseudo-track, due to the charge carriers generated by the photons traversing the bulk of the depleted region, is amplified and time resolved using a wide band oscilloscope. On studying the shape of the induced current one can deduce information of the electric field, doping and charge collection efficiency properties of the detector [8].

The measurements in this study were performed by a Particulars d.o.o. (Ljubljana, Slovenia) based Scanning-TCT setup [9]. Optical excitation was performed with an infrared (IR) laser (λ = 1064 nm) directed on the optical opening in the front side plane of the sensor. The measurements were performed at a low laser intensity equivalent to the charge deposition of 4–5 MIPs, in order to study the effect of charge multiplication due to the gain layer. The reverse bias voltage is applied to the back-plane of the sensor while the transient signal is read from the front side with the n^+ implant. The laser illumination generates charge carriers within the bulk of the active depleted region. Usually in PIN diodes, the transient current signal read out is due to electrons and holes. In case of LGADs, the resulting signal read out by an oscilloscope is a fast signal, mainly due to holes generated by the gain layer that drift to the p^+ electrode (shown in Figure 5 of Ref. [10]). The signal lasts for 2.5 ns due to the sensor thickness (Figure 6 of Ref. [11]).

In addition to the IR laser, the other components in the measurement setup were focusing optics, a sample holder mounted on a XYZ stage for scanning the entire surface of the detector, a Keithley 2410 1100 V Sourcemeter unit, 180 V (maximum allowance) Bias-Tee, a wide band current amplifier with a Tenma power supply, a LeCroy WaveRunner 8404M-MS 4 GHz oscilloscope and a PC and DAQ with LABview based software. The repetition rate of the laser is adjustable from 5 kHz to 500 kHz. In order to obtain the measured interpad-gap profile, the laser was illuminated through the optical opening of the sensors and was scanned across two adjacent pads over 1000 μm with a step size of 2 μm. During the measurement campaign, an average of more than four hundred waveforms were recorded at each scanning point by the oscilloscope.

The laser pulse was transmitted to the detector by an optical fibre. The interpad profile observed in the TCT scan is a convolution of a step function and the Gaussian beam of the IR laser resulting in a S-curve (as shown in Fig. 6a). The curve fitting function is an error-function of the form

$$f(x) = a + \left[\frac{b}{2} \times \mathrm{erf}\left\{\frac{\sqrt{2}(x-c)}{d}\right\}\right] \quad (1)$$

The step ends (= gain layer ends) at 50% of the convolved function relative to its maximum value. This 50% value of the convolved function (S-curve) is determined by parameter c of Eq. (1). We compute the measured interpad-gap width as the distance between the 50% amplitude points of the two interpad profiles (i.e. the distance between 2 gain layers) of adjacent pads [2]. On performing a focus scan, the size of the Gaussian laser spot was determined to be of a magnitude of 25 μm (shown in Fig. 6b), which is much smaller than the size of the optical opening. Therefore, the laser spot is centred within the active area of the sensor.

3.2.1. Measured interpad-gap with varying temperature

The study on temperature dependence of the internal gain of LGADs plays an important role in the sensor performance due to the saturation in drift velocities of charge carriers [12] and the exponential dependence of the impact ionisation rate on temperature [13]. Impact ionisation is a multiplicative phenomena observed in avalanche detectors where they generate a cascade of electron–hole pairs with high drift velocities due to the strong electric fields. Since the impact ionisation of the sensors depends on temperature, a proper understanding of the LGAD functionality with temperature variation is crucial as the gain affects the time resolution as well as the breakdown voltage of the detector [11]. The breakdown due to gain is not a real break of the electric field within the sensor, but it is more related to a multiplication of the dark current [14,15].

Since the gain increases with a decrease in temperature [11], the collected charge increases as the temperature decreases. Fig. 7a shows the pulse shape and amplitude of the signals recorded by the LeCroy oscilloscope as the laser is projected at the optical opening of one of the pads. The amplitude of the signal increases by a factor of 2.5 as the temperature is decreased from 25 °C to −25 °C. This is coherent to the increase in the charge collected due to the gain layer as the laser is projected at the optical opening of the sensor. The normalised value of collected charge increases by a factor of 2.8 as the temperature decreases from 25 °C to −25 °C [16].

The interpad-gap profiles, leakage current values as well as the measured interpad-gap value with temperature variation from 25 °C to −25 °C at a constant bias voltage of 180 V are displayed in Figs. 7b, 7c and 7d, respectively. As expected, the leakage current decreases by nearly two orders of magnitude with a decrease in temperature [16].

As shown in Fig. 8, a positive signal is read out from one of the pads of the sensor when projected with the IR light. Simultaneously, a negative current signal with low amplitude is read out from its adjacent pad. This negative signal observed from the adjacent pad contributes to the negative charge collection values in the measured interpad-gap profiles as shown in Fig. 7b. This observation is due to the charging and discharging of the adjacent pad (similar to that of a capacitor) due to holes, as each of the pads share a common ohmic back-plane.

The measured interpad-gap values and the calculated fill factor of different sensors with varying nominal interpad-gaps are summarised in Table 1. It shows the percentage decrease in the interpad-gap as well as the variation in fill factor with decreasing temperature. The measured interpad-gap for the HPK 3.1 production sensors has an offset of approximately 40 μm from the nominal interpad-gap value. The offset value is constant for all of the sensors with different nominal interpad-gap values. This is coherent to the values measured at room temperature at test beams in Fermi National Accelerator Laboratory, mentioned in the MTD Technical Design Report (TDR) [2]. The fill

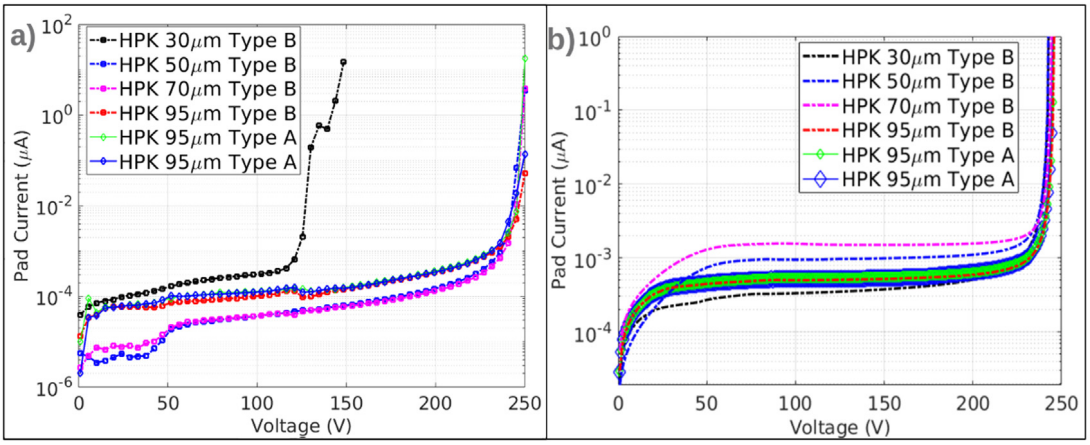

Fig. 5. Current versus voltage plots of HPK 3.1 sensors in two different configurations is shown. In (a) current is readout from one the pads while the three pads are left floating and the common guard ring is grounded, and in (b) current is readout from one of the pads, while the other pads as well as the common guard ring are grounded. Note: All the plots are in logarithmic scale.

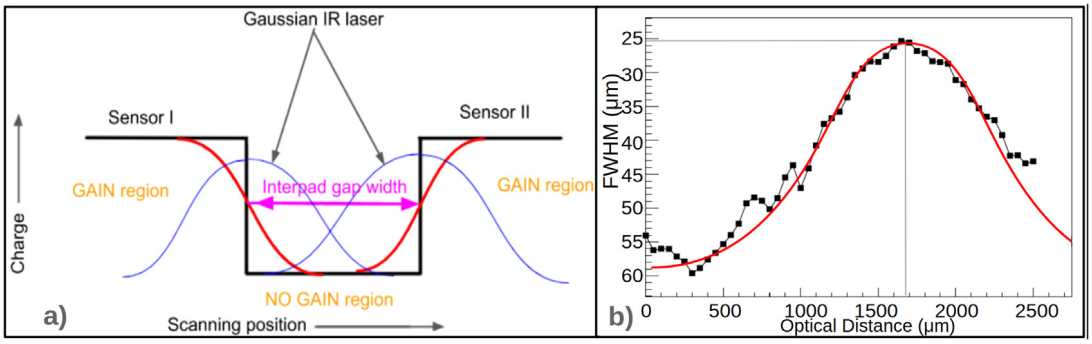

Fig. 6. (a) Measured interpad-gap is the distance between the mid-point of the S-curves of adjacent sensors. (b) FWHM vs optical distance of the IR laser from sensor. Gaussian shape IR spot with size: 25 μm. Focus position of the laser: 1650 μm.

factor values measured at room temperature are consistent with the measured fill factor provided in the MTD TDR [2].

We observe that with a decrease in temperature from 25 °C to −25 °C, the measured interpad-gap decreases by 2–13%. However, the change in the fill factor value is not significant as it increases by about 0.1%.

Due to the temperature dependence of the multiplication layer, the collected charge increases with a decrease in temperature. This leads to an increase in the area of the active region with decreasing temperature. However, when we measure the fill factor with IR laser, the scanned area of the active region is a combination of the charge collected due to the gain region as well as due to the edge effects between the JTE and the ends of gain layer. It is because of the small amount of collected charge arising due to the edges of the p-implant and JTE that we observe a sharp steepness in the slope of the interpad profile (S-curve) as we scan the IR laser across adjacent pads at lower temperatures. Therefore, the decrease in measured interpad-gap values with decreasing temperature is expected because of the increase in the collected charge due to the gain layer; which in turn causes an increase in the slope of the S-curves. As a result of this, the 50% value of the convolved function has a horizontal shift at low temperatures. This explains the decrease in the measured interpad-gap with decreasing temperature.

3.2.2. *Measured interpad-gap with varying proton fluence*

The HPK 3.1 production sensors with different nominal interpad-gap values were irradiated with 10 MeV protons at the IBA cyclone 10/5 cyclotron (Fig. 9a) in the Department of Chemistry at the University of Helsinki [17]. The sensors were placed in a sample holder consisting of collimation slits (of dimensions approximately close to the area of the sensors) such that the integrated current read out from the Keithley 6487 Picoammeter is due to the irradiation of the sensors. The beam profiling was done in such a way that the sample placed under slit 1 and 3 gets an integrated current of 0.15 μA/cm^2 while sensors under slit 2 and 4 (shown in Fig. 9b) of the sample holder receive an integrated current of 0.09 μA/cm^2. The four samples were irradiated simultaneously over 1040 s such that samples in 1 and 3 are irradiated with a fluence of 10^{15} protons/cm^2 while 2 and 4 are irradiated with a fluence of 5×10^{14} protons/cm^2. Total integrated current read out from the four slits was 0.42 μAh. The uniformity of the fluence values for each of the individual slits on the sample holder were cross-checked by performing an autoradiography of a silver foil that was placed under the collimation slits of the sample holder and irradiated at the current values mentioned earlier (shown in Fig. 9b). The sensor with 95 μm nominal interpad-gap irradiated at 10^{15} protons/cm^2 underwent breakdown even at low bias voltages.

The performance of LGADs is affected by the removal of the acceptor atoms in the gain layer of the device [18], as a result of which it worsens the time resolution [19] as well as increases the leakage current due to the bulk which is typical of silicon sensors [20]. This can be observed in Fig. 10c where the leakage current value measured at 180 V at a constant temperature of −25 °C, increases by approximately 2–3 orders of magnitude with an increase in proton fluence. The difference of an order of magnitude in the leakage current for sensors with different nominal interpad-gap irradiated at a given fluence is due to the difference in absolute proton fluence values while irradiating the samples. Further, trapping of charge carriers leads to lower signals (shown in Fig. 10a) and hence the degradation of the spatial resolution and the efficiency (as shown in Fig. 11) [21,22].

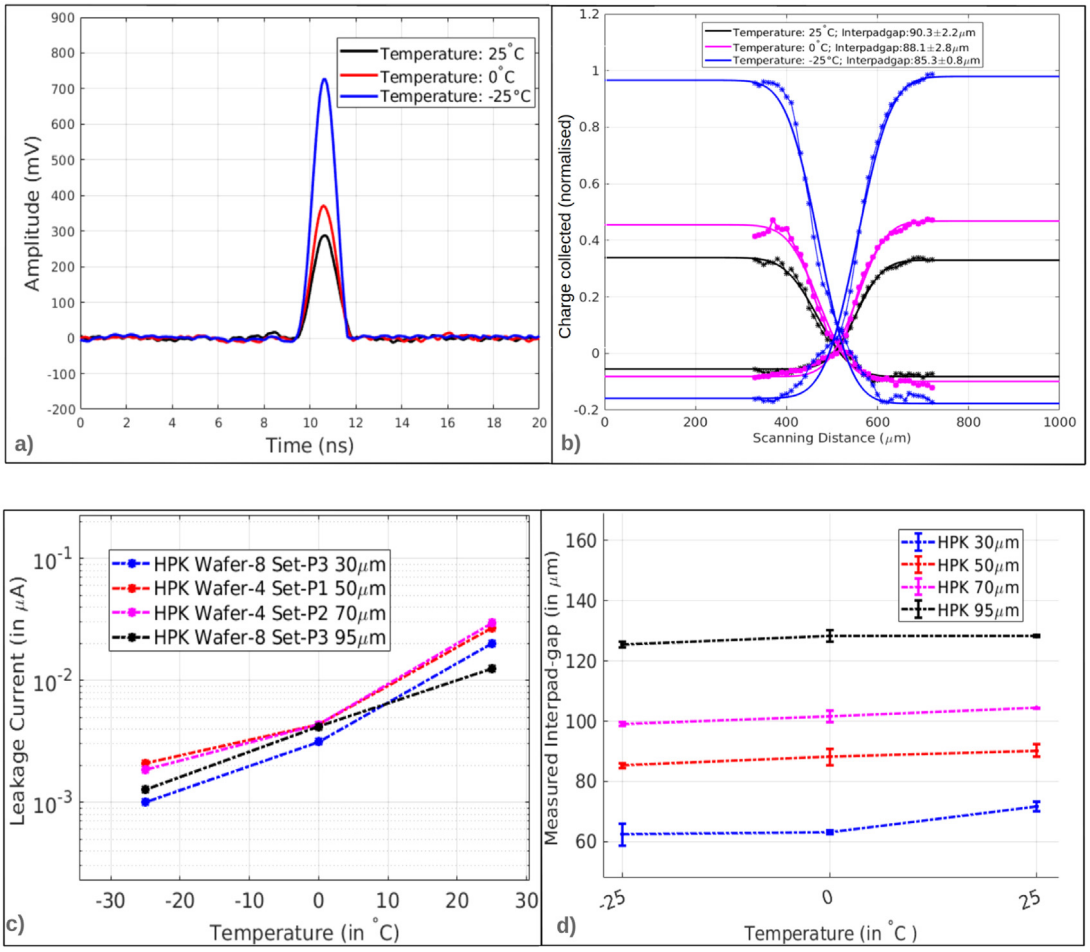

Fig. 7. (a) Pulse shapes, (b) Charge collected (normalised value) vs scanning distance for sensors (at 25 °C, 0 °C and −25 °C) as the laser scans across the two adjacent pads of the sensor with 50 μm nominal interpad-gap, (c) Leakage current with varying temperature and (d) Variation in the measured interpad-gap with temperature. Measurements were performed at a bias voltage of 180 V.

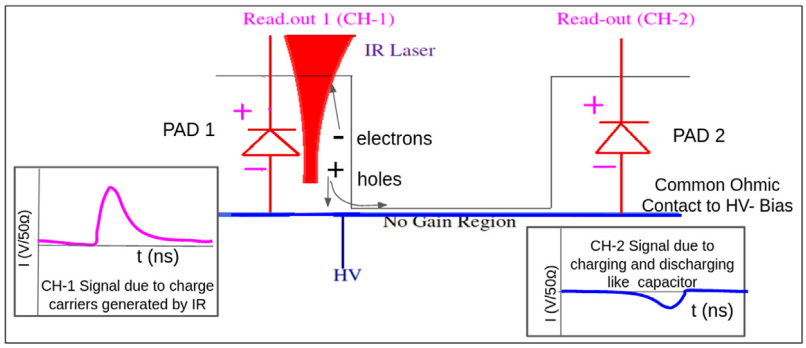

Fig. 8. A diagrammatic representation for explaining the negative current signal observed in adjacent pads as the gain signal is studied when the IR light traverses through one of the pads.

At a fluence of 5×10^{14} protons/cm^2, the interpad-gap is reduced by 20%–40% from its value before irradiation and the collected charge decreases by a factor of 3–4. On irradiating the sensors at 10^{15} protons/cm^2, interpad-gap increases in comparison to its value at 5×10^{14} protons/cm^2 as its charge collection value decreases by a factor of 6. Therefore, on irradiating the sensors at 10^{15} protons/cm^2, the value of the measured interpad-gap decreases by 11%–15% from its value before irradiation. Correspondingly, even though the interpad-gap decreases with an increase in fluence, the fill factor decreases by approximately 1% as the charge collection efficiency (CCE) is worsened due to the effect of irradiation (see Table 2).

The decrease in the interpad-gap with irradiation is due to a combination of: (i) a significant amount of trapping of the multiplication holes within the bulk of the sensor and (ii) a decrease in the signal amplitude which in turn causes a decrease in the amount of charge collected due to the acceptor removal of the gain layer. Before irradiation, there are no deep-level traps within the bulk of the sensor. However, after irradiation, there is a space charge inversion of the p^--layer which causes the depletion region to grow from the back of the sensor towards the front, thereby generating a triple-junction effect within the irradiated sensor [23]. As a result of this distortion in the electric field after irradiation due to trapping of the multiplication holes as well as

Table 1
Variation in the measured interpad-gap and fill factor with temperature at a bias voltage of 180 V.

HPK Sensor (nominal interpad-gap)	Measured interpad-gap of sensor				Fill factor			
	At 25 °C (in μm)	At 0 °C (in μm)	At −25 °C (in μm)	Decrease from 25 °C to −25 °C (in %)	At 25 °C (in %)	At 0 °C (in %)	At −25 °C (in %)	Increase from 25 °C to −25 °C (in %)
30 μm	71.7	63.1	62.4	12.97	89.71	89.73	89.74	0.03
50 μm	90.3	88.1	85.3	5.54	87.62	87.67	87.71	0.09
70 μm	104.3	101.5	99.1	4.98	85.60	85.68	85.69	0.09
95 μm	128.3	128.2	125.5	2.18	82.50	82.52	82.53	0.03

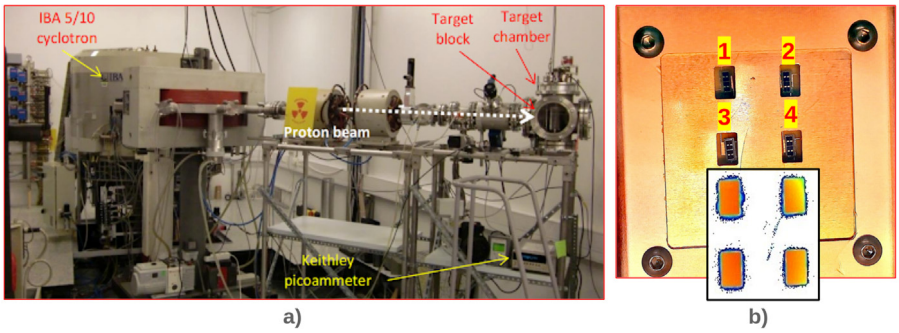

Fig. 9. (a) IBA 10/5 cyclone cyclotron in the Department of Chemistry, (b) Collimator with sample holder showing autoradiograph (using Ag foil) of the beam profile across the four collimation slits.

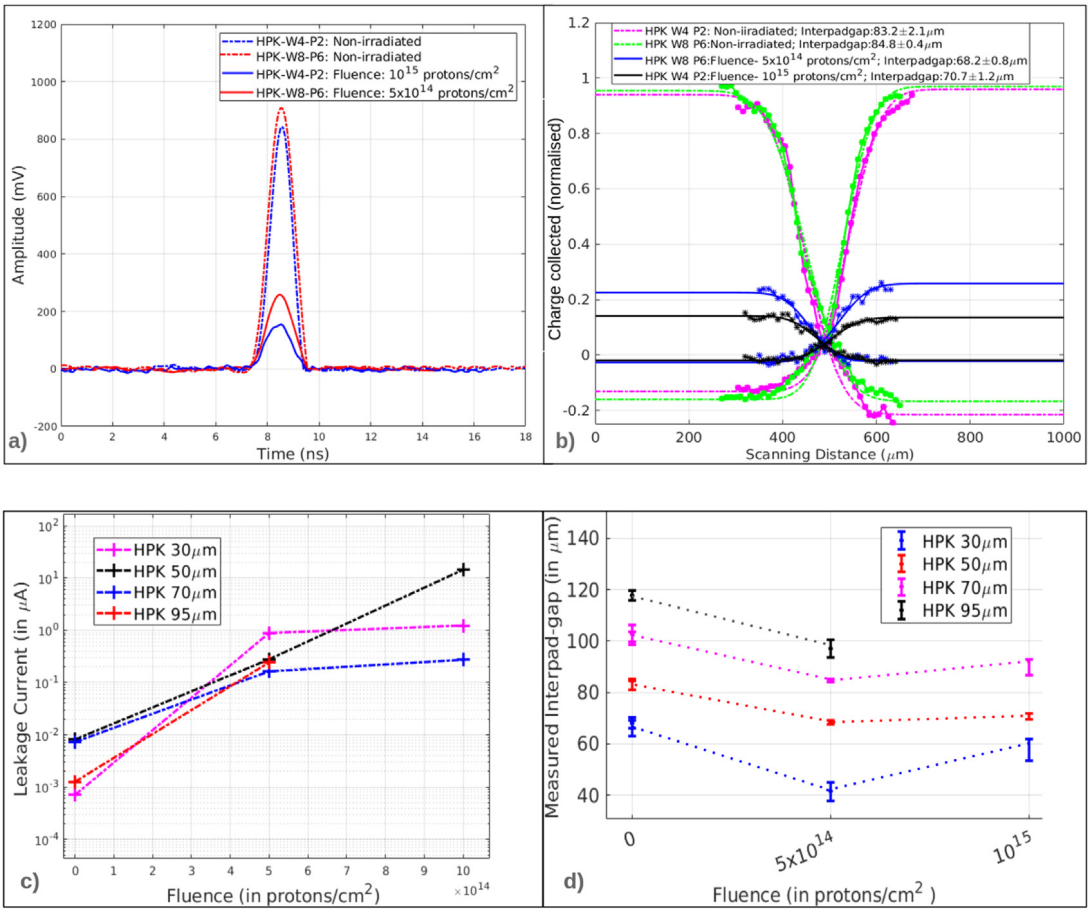

Fig. 10. (a) Pulse shape of non-irradiated and irradiated samples at different proton fluences and (b) Charge Collected (normalised values) vs. scanning distance for sensors as the laser scans across two adjacent pads for sensors with 50 μm interpad-gap. (c) Leakage current with varying fluences and (d) Variation in the measured interpad-gap with proton fluence for sensors with 30, 50, 70 and 95 μm interpad-gap measured at a temperature of −25 °C and 180 V bias voltage.

Table 2
Variation in the measured interpad-gap and fill factor with proton fluence.

HPK Sensor (nominal interpad-gap)	Measured interpad-gap of sensor							
	Un-irradiated (in μm)	Irradiated at 5×10^{14} p/cm^2 (in μm)	% decrease	Decrease in Fill factor (in %)	Un-irradiated (in μm)	Irradiated at 10^{15} p/cm^2 (in μm)	% decrease	Decrease in Fill factor (in %)
30 μm	68.1	41.4	39.21	0.11	66.0	57.6	1.73	0.11
50 μm	84.8	68.2	19.58	0.39	83.2	70.7	15.02	0.25
70 μm	103.0	84.5	17.96	1.41	101.1	89.8	11.18	0.93
95 μm	117.8	97	17.66	0.80	125.0	–	–	–

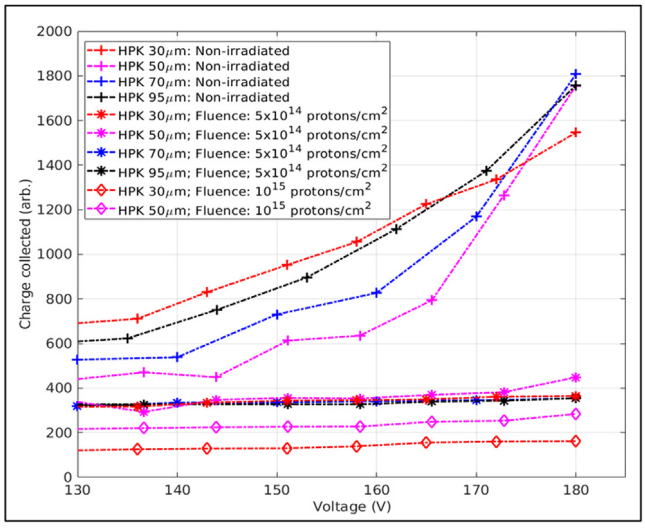

Fig. 11. Voltage scans for the non-irradiated and irradiated samples with varying inter-pad gaps measured at −25 °C.

the decrease in the gain signal amplitude due to the removal of acceptor atoms from the gain layer, the measured interpad-gap decreases with proton irradiation. The decrease in the measured interpad-gap is observed as a result of the decrease in slope of the convolved function and the collected charged values. This explains the horizontal shift in the 50% value of the convolved function and decrease in the measured interpad-gap value of the LGADs on irradiation.

4. Conclusions and summary

Since the fill factor plays a crucial role in determining the performance of the detector, the study of interpad-gap with varying temperature and proton fluence is relevant as the detectors are operated at low temperatures in radiation harsh environment.

The fill factor values for HPK 3.1 LGAD production with different nominal interpad-gaps were measured by varying temperature and irradiating them at different proton fluences. The signal waveform as well as the collected charge of the detectors were studied by recording 1064 nm wavelength IR-laser induced current transients with a TCT measurement set-up. The measurements were performed at 180 V and low laser intensity equivalent to charge deposition of 4–5 MIPs.

Since gain is dependent on temperature, the charge collection increases with a decrease in temperature. Our results show that the measured interpad-gap decreases by 2–12% as the temperature decreases from 25 °C to −25°C. However, the fill factor is not affected significantly by changing temperature as its value increases by approximately 0.1%.

Further, the measured interpad-gap decreases on irradiating the sensors at varying proton fluences. At 10^{15} protons/cm^2, our study shows the measured interpad-gap decreases by 11%–15%. The decrease in the measured interpad-gap is due to a combination of the decrease in the collected charge within the gain region due to acceptor removal of the multiplication layer, since the CCE decreases by a factor of 4–6 with irradiation at high proton fluences, as well as due to trapping of the multiplication holes within the p$^-$-bulk of the detector. However, the fill factor decreases by 0.1–0.9%. This change is not significantly large. Thus, we conclude that the fill factor does not change significantly with temperature and irradiation at varying proton fluences.

Our study has also shown that sensors with 30 μm interpad-gap have a high fill factor but have risks in undergoing an early breakdown when the pads are left floating. For an optimal performance of the ETL for CMS experiment, further studies on the design of LGADs require an optimisation of the gain termination and peripheral regions to prevent early breakdown when not all pads are terminated, while at the same time providing a high fill factor value.

Declaration of competing interest

The authors declare that they have no known competing financial interests or personal relationships that could have appeared to influence the work reported in this paper.

Acknowledgements

The authors are grateful to Dr. Nicolo Cartiglia from Istituto Nazionale di Fisica Nucleare, Universita degli Studi di Torino, Italy and Hamamatsu Photonics K.K, Japan for providing us the sensors for our studies. The research is supported by Magnus Ehrnrooth foundation, Finland. The authors would like to thank Dr. Eija Tuominen, coordinator of the Detector Laboratory, Helsinki Institute of Physics and the Department of Physics, University of Helsinki, for providing the environment for electrical measurements.

References

[1] D. Contardo, M. Klute, J. Mans, L. Silvestris, J. Butler, Technical Proposal for the Phase-2 Upgrade of the Cms Detector, Tech. Rep. CERN-LHCC-2015-010. LHCC-P-008. CMS-TDR-15-02, CERN, Geneva, 2015, https://cds.cern.ch/record/2020886.

[2] C. Collaboration, A MIP Timing Detector for the CMS Phase-2 Upgrade, Tech. Rep. CERN-LHCC-2019-003. CMS-TDR-020, CERN, Geneva, 2019, https://cds.cern.ch/record/2667167.

[3] C. Pena, Precision Timing with the Cms Mip Timing Detector, Tech. Rep. CMS-CR-2018-168, CERN, Geneva, 2018, https://cds.cern.ch/record/2639962.

[4] G. Kramberger, V. Cindro, I. Mandić, M. Mikuž, M. Milovanović, M. Zavrtanik, Modeling of electric field in silicon micro-strip detectors irradiated with neutrons and pions, J. Instrum. 9 (10) (2014) P10016, http://dx.doi.org/10.1088/1748-0221/9/10/p10016.

[5] C. Collaboration, Technical Proposal for a MIP Timing Detector in the CMS Experiment Phase-2 Upgrade, Tech. Rep. CERN-LHCC-2017-027. LHCC-P-009, CERN, Geneva, 2017, https://cds.cern.ch/record/2296612.

[6] P. Fernández-Martínez, D. Flores, S. Hidalgo, V. Greco, A. Merlos, G. Pellegrini, D. Quirion, Design and fabrication of an optimum peripheral region for low gain avalanche detectors, Nucl. Instrum. Methods Phys. Res. A 821 (2016) 93–100, http://dx.doi.org/10.1016/j.nima.2016.03.049, http://www.sciencedirect.com/science/article/pii/S0168900216300663.

[7] F. Hartmann, Evolution of Silicon Sensor Technology in Particle Physics, in: Springer Tracts in Modern Physics, Vol. 275, Springer, 2017, http://dx.doi.org/10.1007/978-3-319-64436-3.

[8] V. Eremin, N. Strokan, E. Verbitskaya, Z. Li, Development of transient current and charge techniques for the measurement of effective net concentration of ionized charges (neff) in the space charge region of p–n junction detectors, Nucl. Instrum. Methods Phys. Res. A 372 (3) (2018) http://dx.doi.org/10.1016/0168-9002(95)01295-8, http://www.sciencedirect.com/science/article/pii/0168900295012958.

[9] Particulars, Advanced measurement systems, Ltd., 2018, [Online], Available: http://www.particulars.si/index.php. (Accessed January 2018).

[10] N. Cartiglia, R. Arcidiacono, M. Baselga, R. Bellan, M. Boscardin, F. Cenna, G.D. Betta, P. Fernndez-Martnez, M. Ferrero, D. Flores, Z. Galloway, V. Greco, S. Hidalgo, F. Marchetto, V. Monaco, M. Obertino, L. Pancheri, G. Paternoster, A. Picerno, G. Pellegrini, D. Quirion, F. Ravera, R. Sacchi, H.-W. Sadrozinski, A. Seiden, A. Solano, N. Spencer, Design optimization of ultra-fast silicon detectors, Nucl. Instrum. Methods Phys. Res. A 796 (2015) 141–148, http://dx.doi.org/10.1016/j.nima.2015.04.025, proceedings of the 10th International Conference on Radiation Effects on Semiconductor Materials Detectors and Devices.

[11] V. Sola, R. Arcidiacono, A. Bellora, et al., Ultra-fast silicon detectors for 4D tracking, J. Instrum. 12 (02) (2017) http://dx.doi.org/10.1088/1748-0221/12/02/c02072.

[12] C. Scharf, R. Klanner, Measurement of the drift velocities of electrons and holes in high-ohmic <100> silicon, Nucl. Instrum. Methods Phys. Res. A 799 (2015) http://dx.doi.org/10.1016/j.nima.2015.07.057, http://www.sciencedirect.com/science/article/pii/S0168900215008955.

[13] C.R. Crowell, S.M. Sze, Temperature dependence of avalanche multiplication in semiconductors, IEEE Trans. Electron Devices ED-13 (8/9) (1966) http://dx.doi.org/10.1109/T-ED.1966.15807.

[14] V. Sola, R. Arcidiacono, M. Boscardin, N. Cartiglia, G.-F.D. Betta, F. Ficorella, M. Ferrero, M. Mandurrino, L. Pancheri, G. Paternoster, A. Staiano, First fbk production of 50 μm ultra-fast silicon detectors, Nucl. Instrum. Methods Phys. Res. A 924 (2019) 360–368, http://dx.doi.org/10.1016/j.nima.2018.07.060, 11th International Hiroshima Symposium on Development and Application of Semiconductor Tracking Detectors.

[15] F. Siviero, Studies of the breakdown in R & D structures of the FBK UFSD3 production, Presentation at RD50 workshop, 2018.

[16] R. Mulargia, Temperature dependence of the response of ultra fast silicon detectors, J. Instrum. 11 (12) (2016) http://dx.doi.org/10.1088/1748-0221/11/12/c12013.

[17] K. Helariutta, et al., The radiochemistry cyclotron in university of Helsinki, Nukleonika 48 (suppl. 2) (2003).

[18] G. Kramberger, et al., Radiation effects in low gain avalanche detectors after hadron irradiations, J. Instrum. 10 (07) (2015) P07006, http://dx.doi.org/10.1088/1748-0221/10/07/p07006.

[19] M. Ferrero, Radiation resistant LGAD design, Nucl. Instrum. Methods Phys. Res. A 919 (2019) http://dx.doi.org/10.1016/j.nima.2018.11.121, http://www.sciencedirect.com/science/article/pii/S0168900218317741.

[20] Z. Galloway, V. Fadeyev, et al., Properties of HPK UFSD after neutron irradiation up to 6e15 n/cm^2, Nucl. Instrum. Methods Phys. Res. A 940 (2019) http://dx.doi.org/10.1016/j.nima.2019.05.017, http://www.sciencedirect.com/science/article/pii/S0168900219306278.

[21] M. Moll, Radiation Damage in Silicon Particle Detectors: Microscopic Defects and Macroscopic Properties (Ph.D. thesis), Hamburg U, 1999, http://www-library.desy.de/cgi-bin/showprep.pl?desy-thesis99-040.

[22] W. Adam, T. Bergauer, et al., Trapping in proton irradiated p$^+$-n-n$^+$ silicon sensors at fluences anticipated at the HL-LHC outer tracker, J. Instrum. 11 (04) (2016) http://dx.doi.org/10.1088/1748-0221/11/04/p04023.

[23] S.O. Ugobono, M. Centis Vignali, M. Fernandez Garcia, C. Gallrapp, S. Hidalgo Villena, I. Mateu, M. Moll, G. Pellegrini, A. Ventura Barroso, I. Vila, Multiplication onset and electric field properties of proton irradiated LGADs, in: 26th International Workshop on Vertex Detectors, 2017, p. 41.